Scheduled Perturbation to Reduce Nondetection Zone for Low Gain Sandia Frequency Shift Method

Mohamed Al Hosani, *Member, IEEE*, Zhihua Qu, *Fellow, IEEE*, and H. H. Zeineldin, *Senior Member, IEEE*

Abstract—It is known that the choice of gain (K) in the Sandia frequency shift (SFS) scheme has direct impacts on the stability of a system with grid-connected distributed generations (DGs). In this paper, a scheduled perturbation technique is proposed to reduce the stability impact of K. In the proposed technique, chopping fraction (cf) is used to compensate for reduction in the value of K, where higher cf values are used to achieve zero nondetection zone (NDZ) under low gain SFS. It is shown by analysis that theoretical reduction of NDZ can be always achieved for a nonzero value of cf. Simulations for single- and multi-DGs systems are performed to verify the analytical analysis. It is shown that an appropriate design of scheduled signal duty cycle (d) is of critical importance to realize the proposed reduction in NDZ. While close synchronization of perturbation signals for multi-DG system is required, a delay of 0.33 s is shown to be tolerated for a two-DG system. Synchronization can be achieved either through locally synchronized timers or by limited communication among DGs. The proposed technique provides an attractive option for systems with high DG penetration by reducing the negative impact of K on stability.

Index Terms—Distributed generation (DG), islanding detection, nondetection zone (NDZ), Sandia frequency shift (SFS).

I. INTRODUCTION

ISLANDING detection schemes have been widely studied recently due to the expected high penetration of distributed generations (DGs) in future distribution networks. It is important for grid-connected inverter-based DGs to be equipped with a reliable islanding detection method (IDM) that allows efficient disconnection of DGs when an islanding condition is detected [1]–[3]. Failure to disconnect unintentionally islanded DGs could compromise the safety of working personnel and/or result in equipment damages. IDMs could be classified into three categories: 1) passive [4]–[9]; 2) active [7]–[10]; and 3) communication-based IDMs [7]. Passive IDMs rely on nonperturbed measurements such as frequency and voltage to detect islanding condition. Over/under frequency protection (OFP/UFP) and over/under voltage protection (OVP/UVP) are examples of commonly used passive methods. On the other hand, a perturbation is used in active IDMs to drift the frequency or voltage beyond certain threshold values. Examples of well-known active IDMs are active frequency drift (AFD), Sandia frequency shift (SFS), and slip-mode frequency shift (SMS). Other active methods rely on injecting negative sequence current and disturbances in either the d-axis or q-axis current controllers to detect an islanding condition [11]–[13]. Several of those techniques such as [11] and [13] require additional control blocks which increases complexity of IDMs. Recently, hybrid IDMs combining the advantages of both passive and active techniques have been proposed in [14]–[16].

Typically, performance of IDMs is evaluated based on the concept of nondetection zone (NDZ) [17]–[25]. NDZ is the region of the appropriately defined load space in which the IDM under investigation fails to detect the islanding condition in a timely manner [17]. The space ($Q_f - f_o$) of RLC load quality factor versus resonant frequency has been proven to be illustrative for AFD and SFS NDZs [19]. In [25], small-signal stability analysis is used to determine the critical Q_f value (Q_f^*) below which the value of Q_f renders unstable islanding operation under SFS. However, application of this technique is time consuming, and an analytical expression of Q_f^* is required. Moreover, the impact of SFS on system stability was studied in [26], and the results showed that high SFS gain (K) might destabilize a grid-connected DG system when the grid is weak or the DG size is large. Hence, it is important to develop a technique that reduces its dependency on gain K to eliminate NDZ. Recently, few studies on applying active IDMs for multi-DG system have been reported in [27]–[30]. For the two-DG case, it was shown in [30] that the use of AFD in one of the DGs will degrade the SFS or SMS performance for the other DG and that the overall NDZ will increase significantly compared to the single DG case. Additionally, it was shown in [31] that the chopping fraction (cf) can be ignored for the SFS IDM since K is more effective in eliminating

M. Al Hosani is with the Department of Electrical Engineering and Computer Science, Masdar Institute, Masdar 54224, UAE (email: mohalhosani@masdar.ac.ae).

H. H. Zeineldin is with the Department of Electrical Engineering and Computer Science, Masdar Institute, Masdar, 54224, UAE, on leave from the Faculty of Engineering, Cairo University, Giza 12316, Egypt (email: hzainaldin@masdar.ac.ae).

Z. Qu is with the Department of Electrical Engineering and Computer Science, University of Central Florida, Orlando, FL 32826 USA (e-mail: qu@ucf.edu).

This article has been accepted for inclusion in a future issue of this journal. Content is final as presented, with the exception of pagination.

2   IEEE TRANSACTIONS ON SMART GRID
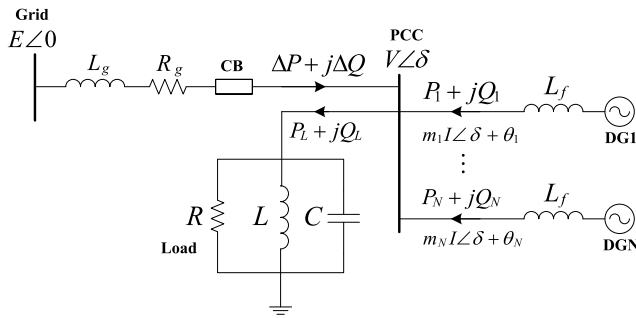

Fig. 1.   Single-line schematic of a multi-DG system.

the NDZ. This paper reveals the role of *cf* in eliminating the NDZ for low gain SFS by employing the concept of scheduled perturbation.

The objective of this paper is to propose a scheduled perturbation IDM where the overall NDZ reduces to the intersection area between two NDZs of two different IDMs. Applying the proposed scheduled perturbation based on one SFS with nonzero *cf* and another SFS with zero *cf* is the case of study considered for this paper. The proposed concept could also be extended to other combinations of IDMs. The *cf* value in SFS plays a major role in eliminating the NDZ for this technique. Hence, this technique will reduce the dependency of *K* to eliminate the NDZ, where zero NDZ, up to a certain value of Q_f, can be obtained through a proper choice of *cf* for low values of *K*. In addition, analytical expressions will be provided to determine the critical values of Q_f for both scheduled perturbation and conventional IDMs.

This paper is organized into four technical sections. Section II presents the DG interface model under study. Design concept and advantages of the scheduled perturbation IDM are introduced in Section III. The performance and synchronization requirements for the proposed technique are tested through simulation for single and two DGs systems and are demonstrated in Section IV. The conclusion is drawn in Section V.

II. SYSTEM UNDER STUDY

A single-line diagram of a general *N*-DG system is shown in Fig. 1, where *N* is the number of connected DGs [25]. In Fig. 1, L_g and R_g are the inductance and resistance of the utility line, respectively. Utility/grid voltage is $E\angle 0$ and the voltage at the point of common coupling (PCC) is $V\angle\delta$. For the *i*th DG, the output power is $P_i + jQ_i$ and the output current is $m_i I\angle\delta + \theta_i$, where *I* is the load current magnitude, m_i is the fraction of load power supplied by the *i*th DG, and θ_i is the positive feedback signal for the *i*th DG unit. The inductance of the inverter filter is represented by L_f and is assumed to be the same for all DGs. The power imbalance between the parallel RLC load and the total power supplied by all DGs is represented by $\Delta P + j\Delta Q$. A circuit breaker (CB) is used to simulate an islanding situation by disconnecting the grid. A three-phase phase-locked loop (PLL) is used to measure the frequency of the PCC voltage. The interface control used for each inverter is a constant current controller. Details of the DG controller and PLL blocks can be found in the Appendix.

III. SCHEDULED PERTURBATION IDM

A. Design Concept

The SFS method is considered as one of the frequency drift methods that attempt to force a positive feedback on the frequency. During a grid connected operation, the system frequency is dictated by the grid frequency. Once the DG is islanded, as a result of the positive feedback, the frequency will drift and hence an islanding condition could be detected. For the conventional SFS method, the positive feedback signal for the *i*th DG is defined as

$$\theta_i = \pi\left(cf_i + K_i\left(f_p - f_g\right)\right)/2 \tag{1}$$

where $i = 1, 2, \ldots, N$, cf_i is the chopping fraction, K_i is the positive feedback gain, f_p is the measured frequency of PCC voltage in Hz, and f_g is the grid base frequency in Hz. Performance of the SFS method will rely on the positive feedback gain value. Higher values of K_i will reduce significantly the NDZ but can lead to DG instability [19], [32].

Let us assume that J_i is the periodic scheduled signal of period T_i to redefine the positive feedback signal for the *i*th DG as follows:

$$\theta_i'(t) = \begin{cases} \theta_i, & 0 < t \le d_i T_i \\ \theta_i^0, & d_i T_i < t \le T_i \end{cases} \tag{2}$$

where $\theta_i^0 = \pi K_i(f_p - f_g)/2$ and d_i is the duty cycle for the periodic perturbation signal J_i. For simplicity, let us assume that the same design parameters (*cf*, *K*, *d*, and *T*) are used for all DGs and hence $\theta_i' = \theta'$. For a multi-DG system ($N \ge 2$), synchronization of scheduled perturbation signals is required. The synchronization can be achieved through one of the following two methods. The first is to provide a local timer to each DG where all timers have to be set in advance to provide the required perturbation signal (*J*). The synchronization requirement can be relaxed as will be seen later in Section IV where a loss of synchronism study will be conducted. Also, the scheduled signal parameters (*d* and *T*) will be chosen in such a way to simplify implementation. The other method is to achieve synchronization through limited communication where d_i information is exchanged among different DGs. This method is more expensive but might be more feasible if some type of communication already exists among DGs [33].

The design objective behind switching perturbation is to obtain an overall NDZ as the intersection area between two different IDMs where scheduling of two SFS techniques will be used to demonstrate effectiveness of the proposed technique. For the conventional SFS method, the phase criterion for determining the NDZ for a single DG system is given as follows [19]:

$$f_o^2 + f_p\frac{\tan(\theta)}{Q_f}f_o - f_p^2 = 0 \tag{3}$$

where f_p is substituted by upper ($f_{\max}$) and lower ($f_{\min}$) threshold values of the OFP/UFP method to determine the upper and lower bounding functions of NDZ, respectively. Fig. 2 shows the NDZs of two SFSs, one corresponding to *cf* = 0 and *K* = 0.02, and the other with *cf* = 0.05 and *K* = 0.02.
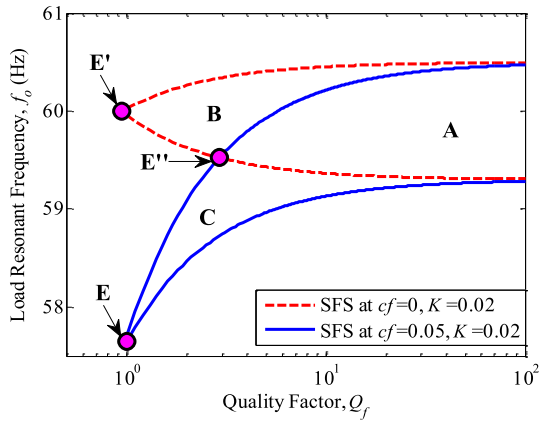
This article has been accepted for inclusion in a future issue of this journal. Content is final as presented, with the exception of pagination.

AL HOSANI *et al.*: SCHEDULED PERTURBATION TO REDUCE NDZ FOR LOW GAIN SFS METHOD 3

Fig. 2. NDZ for SFS at $cf = 0$ and $K = 0.02$ (dashed lines) and SFS at $cf = 0.05$ and $K = 0.02$ (solid lines).
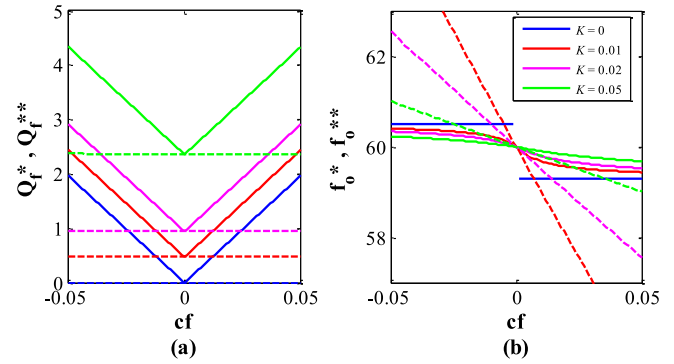

Fig. 3. Effect of cf on (a) Q_f^* (solid lines) and Q_f^{**} (dashed lines) and (b) f_o^* (solid lines) and f_o^{**} (dashed lines) for different K's.

The NDZ for SFS at zero cf is represented by areas **A** and **B** while areas **A** and **C** are the corresponding NDZ for SFS with a nonzero cf value. The SFS critical point, under which any point to the left of this point is unstable, is indicated by point **E** for nonzero cf or point **E′** for zero cf with corresponding coordinate values of Q_f^* and f_o^*, respectively. Let us assume that both d and T are properly designed to provide enough time for both SFSs output frequencies to converge to their steady-state values such that the operating points lying in areas **B** and **C** are considered detectable. Then, area **A** corresponding to the intersection of the two NDZs can be achieved by employing the scheduled perturbation algorithm in (2). Hence, the critical point **E** or **E′** will be shifted to point **E″** which will result in a significant reduction in NDZ by eliminating areas **B** and **C** from NDZs of conventional SFS at zero and nonzero cf values, respectively. The coordinates of point **E″** are Q_f^{**} and f_o^{**}, where Q_f^{**} is always greater than or equal to Q_f^*. This change in NDZ will be studied further in the next two sections.

B. Scheduled Perturbation Effect on Q_f^* and f_o^*

For the conventional SFS method, the equivalent angle for N-DGs can be found as

$$\theta_{\text{eq}} = \tan^{-1}\left(\frac{\sum_{i=1}^{N} m_i \sin\theta_i}{\sum_{i=1}^{N} m_i \cos\theta_i}\right) \tag{4}$$

where θ_{eq} reduces down to θ if common design parameters (i.e., cf and K) are used for all N-DGs. Let us assume that the upper and lower frequency thresholds are f_{max} and f_{min}, respectively. Then, the coordinates of the critical points for

the conventional IDMs can be approximated by

$$Q_f^* \cong \frac{f_g\left(\tan\left(\theta|_{f_p=f_{\text{max}}}\right) - \tan\left(\theta|_{f_p=f_{\text{min}}}\right)\right)}{2\left(f_{\text{max}} - f_{\text{min}}\right)}$$

$$f_o^* \cong \frac{f_{\text{max}}\tan\left(\theta|_{f_p=f_{\text{max}}}\right)}{2Q_f^*}\left[-1 + \sqrt{1 + \left(\frac{2Q_f^*}{\tan\left(\theta|_{f_p=f_{\text{max}}}\right)}\right)^2}\right] \tag{5}$$

where the upper NDZ bounding line is used here to calculate the corresponding f_o^*. In a similar manner, the lower bounding line of NDZ can be used to calculate f_o^*. The result of Q_f^* in (5) was obtained by equating the two NDZ line equations such that the behavior of the RLC load current phase (ϕ_L) was approximated by a Taylor series expansion around $f_p = f_g$ as follows:

$$\tan(\phi_L) \cong \alpha_0 + \alpha_1\left(f_p - f_g\right) \tag{6}$$

where

$$\alpha_0 = Q_f\left(f_g/f_o - f_o/f_g\right)$$
$$\alpha_1 = Q_f\left(1/f_o - f_o/f_g^2\right) \approx 2Q_f/f_g.$$

Similarly, the formulas for calculating Q_f^{**} and f_o^{**} can be obtained. Assuming that both d and T are designed properly, the coordinates of **E″** can be calculated by equating the two equations of NDZ and the results are provided as given in (7), as shown at the bottom of this page. In Fig. 3, the values of both Q_f^* and Q_f^{**} and their corresponding resonant frequencies (f_o^* and f_o^{**}) are shown with respect to cf changes for different K values. For each value of K, Q_f^{**} of scheduled SFS (SSFS) IDM increases linearly as a function of cf while no significant change is noticed for Q_f^*. In other words, the use of cf in the

$$Q_f^{**} \cong \frac{f_g\left(\max\left(\tan\left(\theta|_{f_p=f_{\text{max}}}\right), \tan\left(\theta^0|_{f_p=f_{\text{max}}}\right)\right) - \min\left(\tan\left(\theta|_{f_p=f_{\text{min}}}\right), \tan\left(\theta^0|_{f_p=f_{\text{min}}}\right)\right)\right)}{2\left(f_{\text{max}} - f_{\text{min}}\right)}$$

$$f_o^{**} \cong \frac{f_{\text{max}}\max\left(\tan\left(\theta|_{f_p=f_{\text{max}}}\right), \tan\left(\theta^0|_{f_p=f_{\text{max}}}\right)\right)}{2Q_f^{**}}\left[-1 + \sqrt{1 + \left(\frac{2Q_f^{**}}{\max\left(\tan\left(\theta|_{f_p=f_{\text{max}}}\right), \tan\left(\theta^0|_{f_p=f_{\text{max}}}\right)\right)}\right)^2}\right] \tag{7}$$

This article has been accepted for inclusion in a future issue of this journal. Content is final as presented, with the exception of pagination.

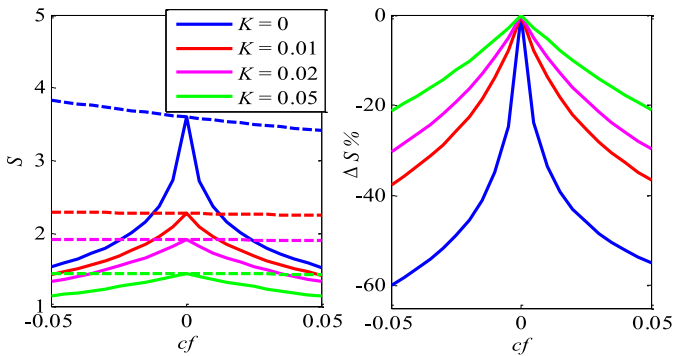4   IEEE TRANSACTIONS ON SMART GRID

Fig. 4.   Size of NDZ for single DG SSFS (solid lines) compared to regular SFS (dashed lines) for different K's.

Fig. 5.   Frequency responses for SSFS IDM. (a) $f_o = 59.4$ Hz, $Q_f = 2.5$, and μ changes. (b) $f_o = 59.56$ Hz, $\mu = 60$, and Q_f changes.

proposed technique always improves the critical values of Q_f and hence the resulting NDZ is reduced. On the other hand, the lower (upper) bound value of f_o^{**} decreases (increases) exponentially as cf value increases, since convergence speed is determined by the value of K and a higher K value corresponds to slower convergence. As cf increases, f_o^{**} converges to the lower or upper thresholds of the OFP/UFP ($f_{\min}$ or $f_{\max}$). In contrast, f_o^* keeps changing linearly as cf increases. It is seen from Fig. 3 that the design condition for a linearly increased Q_f^{**} in the proposed scheme is

$$cf \neq 0. \qquad (8)$$

The condition in (8) can be also obtained by solving the inequality $Q_f^{**} > Q_f^*$ and by utilizing Taylor series expansion of $\tan(\theta)$. Therefore, the proposed use of a nonzero value of cf always results in a higher critical Q_f value, which reduces the overall NDZ, as will be shown next.

C. Reduction of NDZ

The middle point Riemann sum can be used to calculate the NDZ size and is given by [30]

$$S = \sum_{j \in \text{NDZ}} \left(\frac{u(j+1) - u(j)}{2} - \frac{l(j+1) - l(j)}{2} \right)$$
$$\times \left(\log Q_f(j+1) - \log Q_f(j) \right) \qquad (9)$$

where u and l are the upper and lower bounding functions of NDZ, respectively. The log of Q_f is used to emphasize NDZ size for small Q_f values which are of more interest to protection engineers. The relative change of NDZ size is characterized as follows:

$$\Delta S = \frac{S_j - S_k}{S_k} \times 100\% \qquad (10)$$

where S_j is the NDZ size under the SSFS and S_k is the NDZ size under conventional SFS. Let us assume that the NDZ area under investigation is for the values of Q_f from 0.1 to 100 with a step of 0.1. Fig. 4 shows the sizes of NDZs under the SSFS and conventional SFS as a function of cf, as well as the relative changes of NDZ sizes with respect to different K values. The conclusion revealed from Fig. 4 is that the size of NDZ under the proposed scheme is always smaller than that under the conventional SFS method for any nonzero
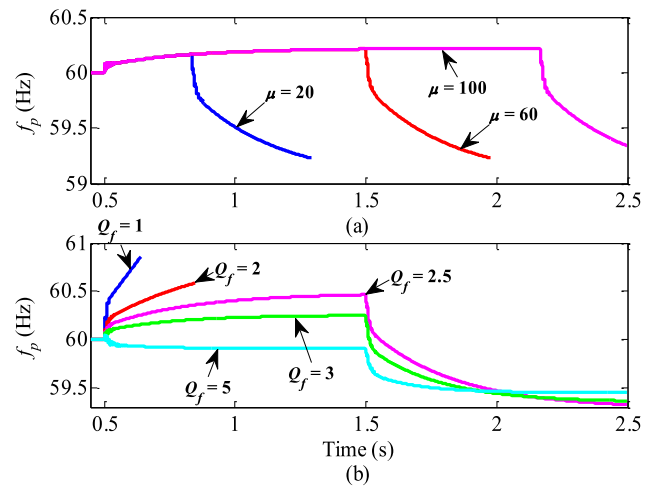
value of cf. Also, a higher NDZ size reduction can be achieved at smaller K, e.g., up to 59.8% reduction in the NDZ size is achieved at $cf = -0.05$ and $K = 0$.

IV. SIMULATION RESULTS

The system, shown in Fig. 1, was modeled in MATLAB/Simulink to verify the theoretical analysis in the preceding sections. For the illustration purpose, the results for both single and multiple ($N = 2$) 10 kW DGs are presented, while the proposed concept can be easily extended for N-DG system. Unless mentioned otherwise, the model parameters in Table II in the Appendix are used in the simulation. The parallel RLC load parameters provided in Table II in the Appendix correspond to a 10 kW load with $f_o = 60$ Hz and $Q_f = 2.5$. For all the cases except for those in Section IV-C, the DG ceases operation if an islanding condition is confirmed by observing that the measured frequency exceeds the threshold values for more than six consecutive cycles. The six cycle delay was proposed in [1] to avoid nuisance tripping due to short-term disturbances.

A. Effect of Duty Cycle

Let us assume that $d_i = \mu_i T_g$, where $T_g = 1/f_g$ is the nominal frequency period and μ_i is the number of cycles perturbed at the ith DG. Standards such as IEEE929-2000 and IEEE1547 require islanding to be detected within less than 2 s of occurrence [1], [3]. Hence, the perturbation signal period for all DGs is assumed to be fixed and equal to 2 s ($T = 2$ s) which corresponds to 120 cycles in 60 Hz. For the single DG case with SSFS IDM, $cf = 0.03957$ and $K = 0.02$ correspond to $Q_f^{**} = 2.5$ as shown in Fig. 3. This is an interesting case to study since conventional SFSs, at relatively low values of K, typically have large NDZs with low Q_f^* values. The reference values used in constant current controller are $i_{d\text{ref}} = 1$ p.u. and $i_{q\text{ref}} = 0$. The CB is opened at $t = 0.5$ s to simulate an islanding condition. In the simulation, the perturbation signal is initiated at $t = 0.5$ s. Fig. 5(a) shows the frequency responses for the SSFS technique at $f_o = 59.4$ Hz and $Q_f = 2.5$ for different μ values. This loading point lies

This article has been accepted for inclusion in a future issue of this journal. Content is final as presented, with the exception of pagination.

AL HOSANI *et al.*: SCHEDULED PERTURBATION TO REDUCE NDZ FOR LOW GAIN SFS METHOD

5

inside the NDZ of SFS with a nonzero *cf* but outside the NDZ of SFS with *cf* being zero and hence is considered to be theoretically detectable by the proposed method. It can be seen that the frequency drifts upward in the first interval due to *cf* and then drifts downward due to the effect of both K and load resonant frequency (59.4 Hz) when *cf* is set to zero for the rest of the cycle. In both cases ($\mu = 20$ and $\mu = 60$), islanding condition is detected since there is sufficient time for SFS with zero *cf* to drift the frequency below $f_{\min}$ and trigger the identification of islanding condition. On the other hand, the deviations in frequency are not significant to detect islanding within 2 s for $\mu = 100$ due to a large duty cycle. Hence, an appropriate choice of μ is critically important to achieve significant reduction in NDZ, as shown in Fig. 4. The choice of μ being 60, which corresponds to a duty cycle of 1 s, will be used for the rest of this paper since it provides adequate time for both SFS techniques to drift the frequency outside the threshold values. Fig. 5(b) shows the frequency responses for SSFS technique at $f_o = 59.56$ Hz and $\mu = 60$ as well as with respect to different Q_f values. These loading points lie on the line of f_o^{**} seen from Fig. 3 for the corresponding *cf* and K values in Table II in the Appendix. All the cases of $Q_f < 2.5$ are detected since they lie outside the NDZ of the proposed technique. The case of $Q_f = 2.5$ corresponds to point $\mathbf{E}''$ in Fig. 2 and is not detectable since the output frequency converges to both upper and lower frequency threshold values without exceeding them. It should be noted that, as the value of Q_f increases, the ability of *cf* term to drift the output frequency becomes less. All the points of $Q_f > 2.5$ are undetectable since they lie inside the NDZ of the proposed technique. It is important to note that the use of nonzero *cf* shifts the critical point toward the upper/lower bound of OFP/UFP. Hence, the value of Q_f that can be detected at $f_o = 60$ Hz is higher than that of Q_f^{**}, and it can be obtained from (3) and is equal to 4.7 for this case. Fig. 6 shows the resulting NDZs under the proposed technique with respect to different μ values. The simulation steps are chosen to be 0.05 Hz for f_o and 0.05 for log Q_f. It can be seen from Fig. 6 that, under the proposed technique, a small duty cycle ($\mu = 20$) results in an NDZ with slower drifting at low Q_f values, when compared to the theoretical NDZ. Therefore, as the duty cycle decreases beyond 20 nominal cycles, the NDZ under the proposed technique converges to the NDZ of SFS with zero *cf*. In comparison, for any large duty cycle ($\mu = 100$), the NDZ converges to the NDZ of SFS with nonzero *cf*. The closest result to the theoretical one was obtained for $\mu = 60$, which corresponds to a duty cycle of half of T, and this result shows why an appropriate choice of duty cycle is critically important.

B. Loss of Synchronism Study for Two-DG System

The purpose of this robustness study is to show how the proposed technique will perform when the two DGs perturbations are not synchronized. Let us assume that we have a two-DG system ($N = 2$) where J_1 is the perturbation signal applied to DG1 and J_2 is the perturbation signal applied to DG2. Assume that J_2 is delayed from J_1 by $L_d T_g$ seconds, where L_d is the number of nominal cycles representing the
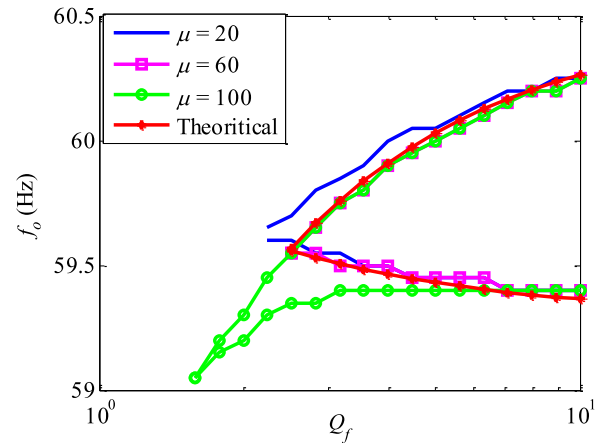

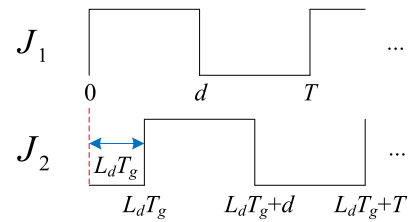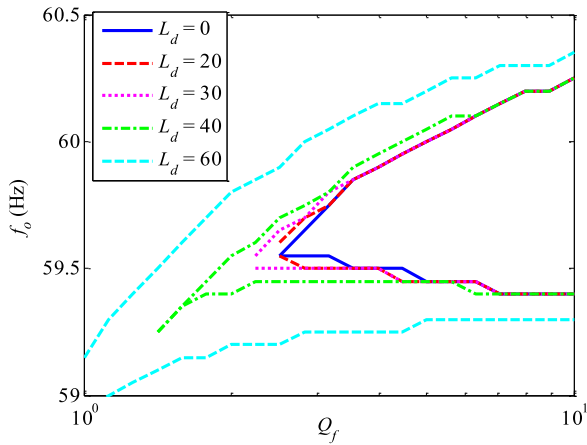Fig. 6. NDZ of SSFS for different duty cycle (μ) values.

Fig. 7. Delayed perturbation signals applied to DG1 and DG2.

delay. Fig. 7 shows the two perturbation signals J_1 and J_2. Assume that parameter values (*cf*, K, d, and T) in Table II in the Appendix are used for both DGs. Also, the load is equally shared by the two DGs such that $i_{dref1} = i_{dref2} = 0.5$ and $i_{qref1} = i_{qref2} = 0$. Fig. 8 shows the effect of delayed cycles (L_d) on the corresponding NDZ under the SSFS technique. For small L_d values ($L_d \leq 20$), there is no significant change in NDZ and therefore, the synchronization requirement for multi-DGs SSFS technique is not strict, where a delay of 0.33 s can be tolerated for $T = 2$ s without any significant degradation of NDZ for a two-DG system. As L_d increases further, the value of Q_f^{**} starts to degrade significantly until no zero NDZ area can be achieved and the resulting NDZ converges to the typical NDZ of two SFS DGs, one at $cf_1 = 0.03957$ and $K_1 = 0.02$ and the other one is at $cf_2 = 0$ and $K_2 = 0.02$, where the load is equally shared between the two DGs (i.e., $m_1 = m_2 = 0.5$). The NDZ when J_1 and J_2 are totally out of synchronism can detect a Q_f value of approximately 2.82 at $f_o = 60$ Hz. Therefore, the performance of a properly designed two-DG system with SSFS would degrade to that of the conventional two-DG SFS if both DGs were completely out of synchronism. This result verifies the advantage of using the proposed simultaneous perturbation technique for multi-DG system rather than alternating one where the later will degrade to OFP/UFP NDZ in the event of a complete loss of synchronism. It is important to note that, for a multi-DG system, all cf_i's should be selected to have the same sign in order to avoid any cancellation effect that could occur when one DG tries to cancel out the perturbation introduced by the other DG [30]. Also, if different design parameters (*cf* or K) are chosen for each DG, then the equivalent angle (θ_{eq}) defined in (4) does
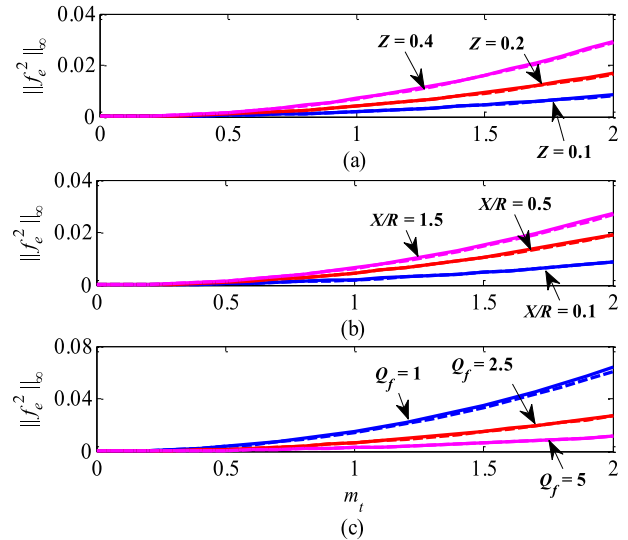
This article has been accepted for inclusion in a future issue of this journal. Content is final as presented, with the exception of pagination.

6   IEEE TRANSACTIONS ON SMART GRID

Fig. 8.   Effect of introduced delay parameter L_d on NDZ.

Fig. 9. $||f_e^2||_\infty$ versus m for single DG (solid) and two DGs (dashed) cases. (a) Z changes. (b) $(X/R)_{\text{ratio}}$ changes. (c) Q_f changes.

not reduce down to θ and the overall NDZ will be dependent upon the output ratios (m_i) of each DG in addition to the SFS parameters [28]. Therefore, it is recommended that, for a multi-DG system, all design parameters (cf, K, d, and T) are chosen to be the same such that the overall NDZ is insensitive of the ratios among different m_i's. These proposed design guidelines make the N-DG system robust against disturbances where no degradation in the overall NDZ will come from losing one or two DGs outputs as long as the rest of DGs can support the active power of the islanded load. However, there is a stability concern related to the total DGs-load share limit as discussed in [26] and [29]. Hence, this issue will be studied in the next section along with the effect of switching perturbation.

C. Sensitivity of Parameters

In order to study the effect of switching perturbation on the frequency response when the grid is connected, the infinity norm of the frequency square error is utilized as the measure. Let us define the frequency error as $f_e = f_p - f_g$, where its norm $||.||_\infty$ corresponds to the maximum square error of switching transition. Value $||f_e^2||_\infty$ versus total DGs-load power share (m_t) will be used to study the effect of different parameters on single and multiple ($N = 2$) DG cases, as shown in Fig. 9. For a single DG case, m_t becomes m_1. The simulation step for m_t is chosen to be 0.05. The load power is assumed to be fixed and, for the two-DG case, both DGs are assumed to supply equal power (i.e., $m_1 = m_2 = m_t/2$). The distribution system line impedance is another important factor that significantly affects f_e. Stronger grid could be represented either by lower impedance magnitude (Z) or lower value of $(X/R)_{\text{ratio}}$. The parameters in Table II in the Appendix correspond to $Z = 0.36$, $(X/R)_{\text{ratio}} = 1.5$, and $Q_f = 2.5$. These parameters are changed one at a time while others are kept constant, and the corresponding values of R_g and L_g can be calculated by

$$R_g = \frac{Z}{\sqrt{1 + (X/R)_{\text{ratio}}^2}}, \quad L_g = \frac{Z(X/R)_{\text{ratio}}}{2\pi f_g \sqrt{1 + (X/R)_{\text{ratio}}^2}}. \quad (11)$$

As seen in Fig. 9, $||f_e^2||_\infty$ increases quadratically as m_t increases, where a higher norm value is obtained as Z or $(X/R)_{\text{ratio}}$ increases to indicate a weaker grid. Also, a higher value of Q_f compresses frequency transition caused by switching and resulted from lower norm values. The results for the two-DG case are slightly smaller than those of the single DG case, and the difference is negligible. Furthermore, other parameters could influence the norm value of frequency error, such as PLL proportional gain (k_{pPLL}), where $||f_e^2||_\infty$ decreases as k_{pPLL} decreases. Another parameter is the load active power (P_L), where a higher P_L value corresponds to a lower load resistance (R) value which results in lower $||f_e^2||_\infty$. Fig. 10 shows $||f_e^2||_\infty$ versus m for a single DG case with respect to different cf and K values. The RLC load was set to $f_o = 60$ Hz and $Q_f = 1$. Fig. 10(a) shows that, as K is kept at 0.05 and cf increases, $||f_e^2||_\infty$ increases quadratically as m increases, where a higher norm value results from higher cf values. On the other hand, Fig. 10(b) shows that, for high K values, there is an upper limit on m after which the system becomes unstable while the grid is still connected. For $K = 0.1$ and 0.2, the system becomes unstable for m higher than 1.65 and 0.8, respectively. These results confirm the outcomes in [26] where a high value of K reduces the maximum allowable share of load power from DGs (m) while cf has no impact on the maximum allowed m. Consequently, there is a tradeoff between choosing such SSFS parameters (cf and K), and the tradeoff effect is between the maximum allowable $||f_e^2||_\infty$ and the required DG-load power share (m). Value $||f_e^2||_\infty$ is proportional to the value of cf, which in turn degrades DG power quality [31]. Therefore, the proposed SSFS technique is very useful for systems with a high penetration of DGs since it reduces the requirements on K and leads to lower negative impact on system stability while the grid is connected.

In the design, the $||f_e^2||_\infty - K$ curve and the $cf - K$ curve are utilized for the proposed technique to meet a certain Q_f^{**}
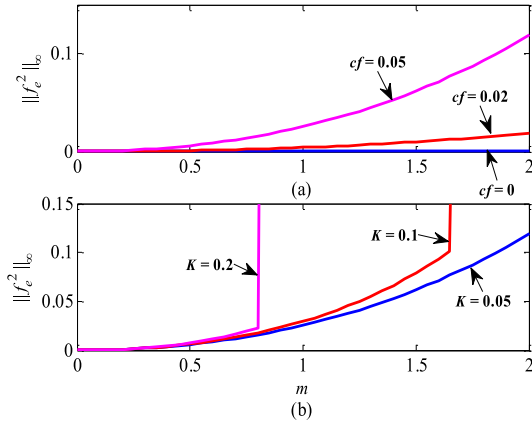
This article has been accepted for inclusion in a future issue of this journal. Content is final as presented, with the exception of pagination.

AL HOSANI *et al.*: SCHEDULED PERTURBATION TO REDUCE NDZ FOR LOW GAIN SFS METHOD

7

Fig. 10. $||f_e^2||_\infty$ versus m for single DG at $Q_f = 1$. (a) $K = 0.05$ and cf changes. (b) $cf = 0.05$ and K changes.
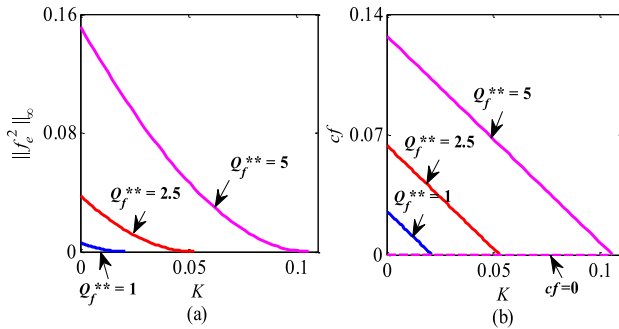

Fig. 11.   (a) $||f_e^2||_\infty - K$ curve. (b) $cf - K$ curve for different Q_f^{**}'s at $Q_f = 1$.

TABLE I
THD RESULTS FOR SFS AND SSFS OF A TWO-DG
SYSTEM WITH AND WITHOUT DELAY

Cases	THD
SFS	3.0107
SSFS at L_k=0	2.7870
SSFS at L_k=20	2.7836
SSFS at L_k=40	2.7865
SSFS at L_k=60	2.7631

value as can be seen in Fig. 11. Let us assume that $Q_f^{**} = 2.5$ is required and the load operating point lies inside $Q_f \geq 1$ region. Hence, the RLC load is set to $Q_f = 1$. The remaining parameters have values given in Table II in the Appendix. For example, if $Q_f^{**} = 2.5$ and $||f_e^2||_\infty \leq 0.02$, then the range of K can be found from Fig. 11(a) to be between 0.0151 and 0.053, which corresponds to cf values between 0.0456 and 0, respectively. This range is limited from the bottom, as shown in Fig. 11(b), by $cf = 0$ line at which no improvement will be obtained from using the SSFS in comparison to the conventional SFS technique.

D. Effect of Proposed SSFS on Power Quality

In this section, a switching Simulink model for a two-DG system is utilized to study the effect of the SSFS technique on power quality of the DGs output current. The current total harmonic distortion (THD) will be used as the measure to study these effects. Table I shows the THD values for SSFS with
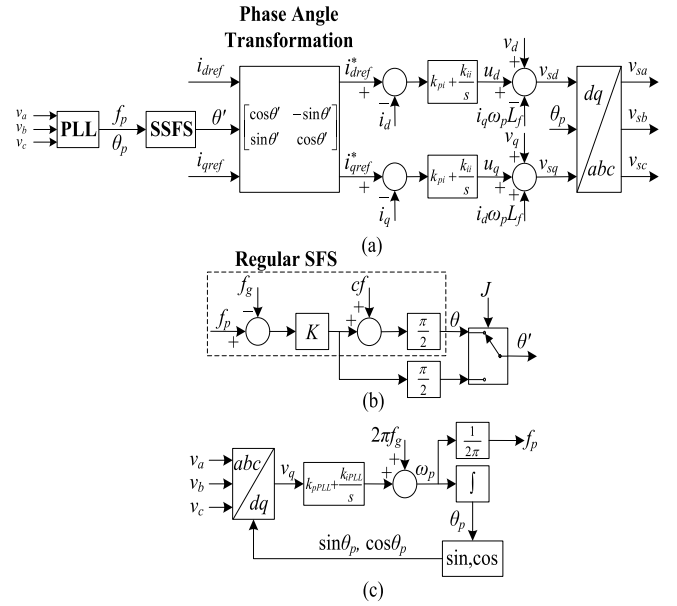

Fig. 12.   Block diagrams of controller and islanding detection circuits of a DG system. (a) Constant current controller. (b) SSFS. (c) Three-phase PLL.

TABLE II
SIMULATION PARAMETERS

Parameters	Value	Parameters	Value
$V_{(phase\ to\ ground)}$	120 V	R	4.32 Ω
V_{dc}	600 V	L	4.5837 mH
V_{base}, S_{base}	170 V, 10 kVA	C	1.5351 mF
f_g	60 Hz	k_{pi}, k_{ii}	0.5, 500
f_{min}, f_{max}	59.3, 60.5 Hz	k_{pPLL}, k_{iPLL}	50, 500
R_g, L_g	0.2 Ω, 0.796 mH	cf, K	0.03957, 0.02
L_f	3 mH	d, T	1 s, 2 s

respect to different delays in comparison to the conventional SFS results. The first 40 harmonics are used for calculating THD [3]. The remaining parameters are the same as those in Table II in the Appendix except that the RLC load parameters are set to 20 kW with $f_o = 60$ Hz and $Q_f = 2.5$. Also, the load power is equally shared by the two DGs such that $i_{dref1} = i_{dref2} = 1$ and $i_{qref1} = i_{qref2} = 0$. The switching frequency of inverter is set to 8 kHz. The results in Table I show that the proposed technique results in a reduction in the THD value when compared to the conventional SFS technique. This is another advantage of the proposed technique since scheduling between two SFSs, one with zero cf and the other with nonzero cf, reduces the THD value and hence enhances the overall power quality of DG outputs while improving NDZ.

V. CONCLUSION

In this paper, a scheduled perturbation method of islanding detection is developed to reduce the dependency on SFS gain K in eliminating NDZ. The cf is increased as the alternative to eliminate NDZ, and the removal of NDZ is achieved for SSFS with zero gain. An analytical formula for critical Q_f value is obtained for both regular and scheduled perturbation IDMs. For a single DG system, simulation results show that appropriate selection of scheduled signal duty cycle is the key to accomplish the theoretical NDZ reduction under the

This article has been accepted for inclusion in a future issue of this journal. Content is final as presented, with the exception of pagination.

8

IEEE TRANSACTIONS ON SMART GRID

proposed method. It is also shown that, while synchronization is needed for a multi-DG system, a maximum delay of 0.33 s can be tolerated for a two-DG system without impacting upon NDZ. The $||f_e^2||_\infty - K$ and $cf - K$ curves are provided for making right choices of parameters in order to achieve a certain critical value of Q_f while ensuring that the frequency error in norm is under a certain bound. In addition, the proposed technique improves the overall power quality of DG outputs by reducing the THD. The proposed technique would be useful particularly for systems with high DG penetration because the negative impact of SFS gain on stability is now alleviated.

APPENDIX

The constant current controller implemented for a DG system is shown in Fig. 12(a). Symbols $i_{d\text{ref}}$ and $i_{q\text{ref}}$ are the d- and q-axis DG output current references, respectively. A phase angle transformation is applied to obtain new current references $i_{d\text{ref}}^*$ and $i_{q\text{ref}}^*$. The angle θ' used in transformation is the output of SSFS IDM introduced in Fig. 12(b), where the conventional SFS output is applied to a multi-input single-output switch, which is driven by a scheduled signal J, to obtain θ'. The other input of the switch is an SFS output with zero cf. The input frequency to SSFS is measured by a three-phase PLL as shown in Fig. 12(c). Then, the new references are subtracted from measured output currents (i_d and i_q) and applied to proportional-integral controllers with gains k_{pi} and k_{ii}, respectively. Finally, a dq–abc transformation is applied to construct three-phase voltage signals (v_{sa}, v_{sb}, and v_{sc}) which will be used to drive the controlled voltage sources as illustrated in Fig. 1. The parameters used in the simulation studies are given in Table II.

REFERENCES

[1] *IEEE Recommended Practice for Utility Interface of Photovoltaic (PV) Systems*, IEEE Standard 929–2000, Apr. 2000.

[2] *Inverters, Converters, and Controllers for Use in Independent Power Systems*, UL Standard 1741, 2002.

[3] *IEEE Application Guide for IEEE Standard 1547, IEEE Standard for Interconnecting Distributed Resources With Electric Power Systems*, IEEE Standard 1547.2-2008, Apr. 2009.

[4] A. Samui and S. Samantaray, "Assessment of ROCPAD relay for islanding detection in distributed generation," *IEEE Trans. Smart Grid*, vol. 2, no. 2, pp. 391–398, Jun. 2011.

[5] H. Far, A. Rodolakis, and G. Joos, "Synchronous distributed generation islanding protection using intelligent relays," *IEEE Trans. Smart Grid*, vol. 3, no. 4, pp. 1695–1703, Dec. 2012.

[6] F. De Mango, M. Liserre, and A. Aquila, "Overview of anti-islanding algorithms for PV systems. Part I: Passive methods," in *Proc. 12th Int. Power Electron. Motion Control Conf.*, Portorož, Slovenia, Sep. 2006, pp. 1878–1883.

[7] W. Bower and M. Ropp, "Evaluation of islanding detection methods for photovoltaic utility-interactive power systems," Int. Energy Agency, Paris, France, Tech. Rep. IEA-PVPS T5-09, Mar. 2002.

[8] G. Petrone, R. Spagnuolo, M. Teodorescu, and M. Veerachary, "Reliability issues in photovoltaic power processing systems," *IEEE Trans. Ind. Electron.*, vol. 55, no. 7, pp. 2569–2580, Jul. 2008.

[9] B. Yu, M. Matsui, and G. Yu. (2010). *A Review of Current Anti-Islanding Methods for Photovoltaic Power System*. [Online]. Available: http://www.sciencedirect.com/science/article/pii/S0038092X10000319

[10] F. De Mango, M. Liserre, and A. Aquila, "Overview of anti-islanding algorithms for PV systems. Part II: Active methods," in *Proc. 12th Int. Power Electron. Motion Control Conf.,* Portorož, Slovenia, Sep. 2006, pp. 1884–1889.

[11] H. Karimi, A. Yazdani, and R. Iravani, "Negative sequence current injection for fast islanding detection of a distributed resource unit," *IEEE Trans. Power Electron.*, vol. 23, no. 1, pp. 298–307, Jan. 2008.

[12] Z. Ye *et al.*, "Study and development of anti-islanding control for grid-connected inverters," Nat. Renew. Energy Lab., Golden, CO, USA, Tech. Rep. NREL/SR-560-36243, May 2004.

[13] G. Gonzalez and R. Iravani, "Current injection for active islanding detection of electronically-interfaced distributed resources," *IEEE Trans. Power Del.*, vol. 21, no. 3, pp. 1698–1705, Jul. 2006.

[14] V. Menon and M. Nehrir, "A hybrid islanding detection technique using voltage unbalance and frequency set point," *IEEE Trans. Power Syst.*, vol. 22, no. 1, pp. 442–448, Feb. 2007.

[15] P. Mahat, Z. Chen, and B. Jensen, "A hybrid islanding detection technique using average rate of voltage change and real power shift," *IEEE Trans. Power Del.*, vol. 24, no. 2, pp. 764–771, Apr. 2009.

[16] P. Ray, N. Kishor, and S. Mohanty, "Islanding and power quality disturbance detection in grid-connected hybrid power system using wavelet and S-transform," *IEEE Trans. Smart Grid*, vol. 3, no. 3, pp. 1082–1094, Sep. 2012.

[17] M. Ropp *et al.*, "Determining the relative effectiveness of islanding detection methods using phase criteria and nondetection zones," *IEEE Trans. Energy Convers.*, vol. 15, no. 3, pp. 290–296, Sep. 2000.

[18] Z. Ye, A. Kolwalkar, Y. Zhang, P. Du, and R. Walling, "Evaluation of anti-islanding schemes based on nondetection zone concept," *IEEE Trans. Power Electron.*, vol. 19, no. 5, pp. 1171–1176, Sep. 2004.

[19] L. Lopes and H. Sun, "Performance assessment of active frequency drifting islanding detection methods," *IEEE Trans. Energy Convers.*, vol. 21, no. 1, pp. 171–180, Mar. 2006.

[20] A. Roscoe, G. Burt, and C. Bright, "Avoiding the NDZ of passive loss-of-mains (islanding) relays for synchronous generation by using low bandwidth control loops and controlled reactive power mismatches," *IEEE Trans. Smart Grid*, vol. 5, no. 2, pp. 602–611, Mar. 2014.

[21] J. Vieira, W. Freitas, W. Xu, and A. Morelato, "An investigation on the nondetection zones of synchronous distributed generation anti-islanding protection," *IEEE Trans. Power Del.*, vol. 23, no. 2, pp. 593–600, Apr. 2008.

[22] H. Zeineldin and J. Kirtley, "Performance of the OVP/UVP and OFP/UFP method with voltage and frequency dependent loads," *IEEE Trans. Power Del.*, vol. 24, no. 2, pp. 772–778, Apr. 2009.

[23] H. Zeineldin and M. Salama, "Impact of load frequency dependence on the NDZ and performance of the SFS islanding detection method," *IEEE Trans. Ind. Electron.*, vol. 58, no. 1, pp. 139–146, Jan. 2011.

[24] B. Bahrani, H. Karimi, and R. Iravani, "Nondetection zone assessment of an active islanding detection method and its experimental evaluation," *IEEE Trans. Power Del.*, vol. 26, no. 2, pp. 517–525, Apr. 2011.

[25] X. Wang, W. Freitas, and W. Xu, "Dynamic non-detection zones of positive feedback anti-islanding methods for inverter-based distributed generators," *IEEE Trans. Power Del.*, vol. 26, no. 2, pp. 1145–1155, Apr. 2011.

[26] X. Wang and W. Freitas, "Impact of positive-feedback anti-islanding methods on small-signal stability of inverter-based distributed generation," *IEEE Trans. Energy Convers.*, vol. 23, no. 3, pp. 923–931, Sep. 2008.

[27] L. Lopes and Y. Zhang, "Islanding detection assessment of multi-inverter systems with active frequency drifting methods," *IEEE Trans. Power Del.*, vol. 23, no. 1, pp. 480–486, Jan. 2008.

[28] H. Zeineldin and S. Conti, "Sandia frequency shift parameter selection for multi-inverter systems to eliminate non-detection zone," *IET Renew. Power Gener.*, vol. 5, no. 2, pp. 175–183, Mar. 2011.

[29] X. Wang, W. Freitas, V. Dinavahi, and W. Xu, "Investigation of positive feedback anti-islanding control for multiple inverter-based distributed generators," *IEEE Trans. Power Syst.*, vol. 24, no. 2, pp. 785–795, May 2009.

[30] E. Estebanez, V. Moreno, A. Pigazo, M. Liserre, and A. Aquila, "Performance evaluation of active islanding-detection algorithms in distributed-generation photovoltaic systems: Two inverters case," *IEEE Trans. Ind. Electron.*, vol. 58, no. 4, pp. 1185–1193, Apr. 2011.

[31] H. Zeineldin and S. Kennedy, "Sandia frequency-shift parameter selection to eliminate nondetection zones," *IEEE Trans. Power Del.*, vol. 24, no. 1, pp. 486–487, Jan. 2009.

[32] H. Vahedi, M. Karrari, and G. Gharehpetian, "Accurate SFS parameter design criterion for inverter-based distributed generation," *IEEE Trans. Power Del.*, in press.

[33] H. Xin, Z. Qu, J. Seuss, and A. Maknouninejad, "A self-organizing strategy for power flow control of photovoltaic generators in a distribution network," *IEEE Trans. Power Syst.*, vol. 26, no. 3, pp. 1462–1473, Aug. 2011.

Mohamed Al Hosani (S'10–M'13) received the B.Sc. degree in electrical engineering from the American University of Sharjah, Sharjah, UAE, in 2008, and the M.Sc. and Ph.D. degrees in electrical engineering from the University of Central Florida, Orlando, FL, USA, in 2010 and 2013, respectively.

He is currently an Assistant Professor with Masdar Institute, Masdar, UAE. His current research interests include anti-islanding algorithm, distributed generation protection and control, and microgrid stability analysis.

Zhihua Qu (M'90-SM'93-F'10) received the Ph.D. degree in electrical engineering from the Georgia Institute of Technology, Atlanta, GA, USA, in 1990.

He has been with the University of Central Florida (UCF), Orlando, FL, USA. Currently, he is a Pegasus Professor at UCF, the SAIC Endowed Professor at the College of Engineering and Computer Science, a Professor and the Chair of Electrical and Computer Engineering, and the Director of the FEEDER Center (Foundations for Engineering Education for Distributed Energy Resources, a US Department of Energy funded consortia on distributed technologies and smart grid). His areas of expertise are nonlinear systems and control with applications to energy and power systems. In energy systems, his research covers such subjects as low-speed power generation, dynamic stability of distributed power systems, anti-islanding control and protection, distributed generation and load sharing control, distributed VAR compensation, distributed optimization, and cooperative control.

H. H. Zeineldin (M'08–SM'13) received the B.Sc. and M.Sc. degrees in electrical engineering from Cairo University, Giza, Egypt, in 1999 and 2002, respectively, and the Ph.D. degree in electrical and computer engineering from the University of Waterloo, Waterloo, ON, Canada, in 2006.

He was with Smith and Andersen Electrical Engineering, Inc., North York, ON, Canada, where he was involved with projects involving distribution system design, protection, and distributed generation. He was a Visiting Professor with the Massachusetts Institute of Technology, Cambridge, MA, USA. He is with the Faculty of Engineering, Cairo University. He is currently an Associate Professor with the Masdar Institute of Science and Technology, Masdar, UAE. His current research interests include power system protection, distributed generation, and microgrids.

Dr. Zeineldin is currently an Editor of the IEEE TRANSACTIONS ON ENERGY CONVERSION and the IEEE TRANSACTIONS ON SMART GRIDS.